Bayesian Tensor Filtering: Smooth, Locally-Adaptive Factorization of Functional Matrices

Wesley Tansey[*][1,2], Christopher Tosh[1], and David M. Blei[1,3,4]

[1]Data Science Institute, Columbia University, New York, NY, USA
[2]Department of Systems Biology, Columbia University Medical Center, New York, NY, USA
[4]Department of Statistics, Columbia University, New York, NY, USA
[5]Department of Computer Science, Columbia University, New York, NY, USA

Abstract

We consider the problem of functional matrix factorization, finding low-dimensional structure in a matrix where every entry is a noisy function evaluated at a set of discrete points. Such problems arise frequently in drug discovery, where biological samples form the rows, candidate drugs form the columns, and entries contain the dose-response curve of a sample treated at different concentrations of a drug. We propose Bayesian Tensor Filtering (BTF), a hierarchical Bayesian model of matrices of functions. BTF captures the smoothness in each individual function while also being locally adaptive to sharp discontinuities. The BTF model is agnostic to the likelihood of the underlying observations, making it flexible enough to handle many different kinds of data. We derive efficient Gibbs samplers for three classes of likelihoods: (i) Gaussian, for which updates are fully conjugate; (ii) Binomial and related likelihoods, for which updates are conditionally conjugate through Pólya–Gamma augmentation; and (iii) Black-box likelihoods, for which updates are non-conjugate but admit an analytic truncated elliptical slice sampling routine. We compare BTF against a state-of-the-art method for dynamic Poisson matrix factorization, showing BTF better reconstructs held out data in synthetic experiments. Finally, we build a dose-response model around BTF and show on real data from a multi-sample, multi-drug cancer study that BTF outperforms the current standard approach in biology. Code for BTF is available at `https://github.com/tansey/functionalmf`.

1 Introduction

To search for new therapeutics, biologists carry out exploratory studies of drugs. They test multiple drugs, at different doses, against multiple biological samples

[*] `wesley.tansey@columbia.edu` (corresponding author)

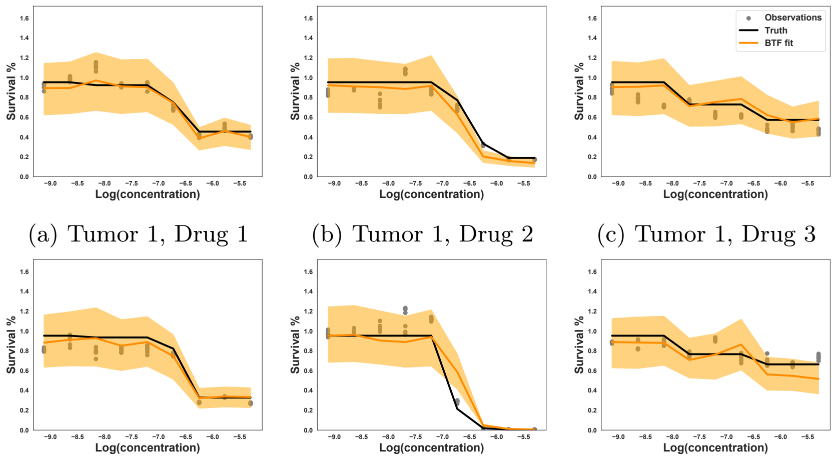

(a) Tumor 1, Drug 1 (b) Tumor 1, Drug 2 (c) Tumor 1, Drug 3

(d) Tumor 2, Drug 1 (e) Tumor 2, Drug 2 (f) Tumor 2, Drug 3

Figure 1: Sample of data from a simulated cancer drug experiment with correlated errors and heteroskedastic observation noise. Bands represent 50% posterior predictive credible intervals for observations.

(e.g., different tumors). The goal is to trace the dose-response curves, and to understand the efficacy of each drug.

The experiments in such dose-response studies are costly; each one can take weeks or months to conduct in the lab. Consequently, a good predictive model of dose-response is useful as a tool for interactive experimental design. With a predictive model, biologists can prioritize some experiments over others based on its predictions and its levels uncertainty around them.

Figure 1 shows a simulated study about cancer drug discovery.[1] Each panel illustrates the interaction of one type of drug with one type of tumor. The black line illustrates the true dose-response curve for that drug and that tumor, and the gray points simulate a set of experiments, each set with 6 replicates measured at 9 different doses. The goal is to use the observations (gray points) to predict the true dose-response curves (black lines). In Figure 1, those predictions—the orange lines and uncertainty bands—come from Bayesian tensor filtering (BTF), the method we propose in this paper.

Notice there is relational structure in the outcomes: each drug has similar effects on both tumors. Thus, we treat predictive modeling of dose-response as a factorization problem. The relational structure in the data arises because tumors share latent molecular attributes, such as genomic mutations, and drugs share latent pharmaceutical attributes, such as chemical structures. In each experiment, tumor and drug attributes interact, creating the shared patterns of dose-response.

While traditional factorization considers a matrix of scalars, the entries of

[1] Privacy concerns prevent us from plotting real data; we analyze a real dataset in Section 5.

this matrix are latent dose-response curves subsampled at different doses. To model such curves, we model drug attributes as changing functions of dose. Moreover, while the effects usually vary smoothly, there are occasional sharp jumps, such as between the fifth and sixth dose levels of drug 2. Capturing latent structure in dose-response curves requires handling this type of non-stationarity.

As a final wrinkle, depending on the drugs being tested, equipment being used, or samples under study, the types of observations will change. Some studies may generate count data for the number of cells surviving; others measure a real-valued metric of cell health or survival. In the case of cancer, drugs are chosen that will only kill cells, not facilitate growth; effects in these curves are therefore upper bounded. All of these complexities mean that good models of dose-response curves must handle many different likelihoods and allow the scientist to encode biological constraints on parameter values.

Bayesian tensor filtering (BTF) is a probabilistic method for functional matrix factorization that handles these special properties of data about dose-response curves. BTF uses structured shrinkage priors that encourage smoothness in the estimated functions; it is locally adaptive, enabling the functions to make sharp jumps when the data calls for it; and it can accommodate any likelihood function. We derive efficient MCMC inference methods for BTF: specialized inference for the Gaussian and binomial likelihoods, and a new inference method called generalized analytic slice sampling (GASS), for more general likelihoods. BTF enables us to develop a new state-of-the-art method for dose-response modeling in cancer drug studies.

Contributions. This paper makes the following contributions: (i) Bayesian tensor filtering, a flexible model for functional matrix factorization (Section 2); (ii) generalized analytic slice sampling, a procedure for sampling from posteriors with constrained multivariate normal priors and non-conjugate likelihoods (Section 3); and (iii) a new Bayesian dose-response model for multi-drug, multi-sample cancer studies, built on top of BTF and GASS (Section 4). In Section 5 we empirically study BTF. We compare it to a state-of-the-art method for functional Poisson matrix factorization and find it better models non-stationary functional matrices. We also study the dose-response model on a real cancer dataset and find it has better reconstruction performance than standard approaches used in the dose-response literature.

Related work. We survey a collection of the most relative work to the BTF model. Much more work has been done on many of the components in BTF. We refer the reader to Bhadra et al. [2] for a more complete survey on horseshoe shrinkage in complex models. For an overview of trend filtering, see Tibshirani [23]; see Faulkner and Minin [7] for a Bayesian extension.

Bayesian factor modeling. Many models have been developed for Bayesian factor analysis with smooth structure. Zhang and Paisley [28] apply a group lasso penalty to the rows and columns of a matrix then derive a variational EM algorithm for inference. Hahn et al. [10] use horseshoe priors for sparse Bayesian factor analysis in causal inference scenarios with many instrumental variables. Kowal et al. [12] develop a time series factor model using a Bayesian trend filtering prior on top of a linear dynamical system with Pólya–Gamma augmentation for binomial observations. Schein et al. [18] develop poisson-gamma dynamical systems (PGDS), a dynamic matrix factorization model specifically for poisson-distributed observations; we compare BTF with a tensor extension of PGDS in Section 5. Unlike the above models, BTF is likelihood-agnostic through GASS inference and enables modeling of independently-evolving columns rather than a common time dimension.

Dose-response modeling. Inferring the effects of a drug on biological samples is a common task in biology. The state of the art is a logistic factor model [25]. In large-scale studies [e.g., 8], hundreds of thousands of experiments are conducted automatically via robots over a series of years. When such massive datasets are available, deep learning methods have been shown to improve dose-response modeling [22]. The focus of the BTF dose-response model is on pilot studies conducted in the lab by scientists, where often the techniques being used are too new to be scaled up via robots or the samples being experimented on require expert preparation that cannot be automated. This is the case, for instance, in many oragnoid experiments [5]; our case study in Section 5 is on an organoid dataset.

2 Bayesian tensor filtering for functional matrix factorization

Let $Y \in \mathbb{R}^{N \times M \times T \times R}$ be an $N \times M$ matrix of noisy functions evaluated at T points, with each point observed R times. The goal in functional matrix factorization is to leverage the relational structure between entries to denoise the observations and predict missing functions. We develop Bayesian tensor filtering (BTF), a hierarchical model of functional matrices. Since our main application is dose-response modeling, we describe BTF in terms of Y being a matrix of N biological samples tested against M drugs, each at T doses with R replicates.

Latent attributes for biological samples. Biological samples in a study will share molecular attributes. In cancer, different tumor samples will contain similar patterns of genomic mutations, copy number alterations, and gene expression [26]. In mixed tissue experiments, cells that have differentiated into the same type will often respond similarly [e.g., 11]. These attributes are captured in BTF with a latent vector, $w_i \in \mathbb{R}^D$ for the i^{th} sample, as in standard matrix factorization,

$$w_i \sim \text{MVN}(\mathbf{0}, \sigma^2 I)\,, \qquad \sigma^{-2} \sim \text{Gamma}(0.1, 0.1)\,. \tag{1}$$

The choice of the embedding size, D, is a hyperparameter.

Latent dose-specific attributes for drugs. For the j^{th} column in the functional matrix, BTF models an entire curve $V_j \in \mathbb{R}^{T \times D}$. Intuitively, we expect the effects to mostly vary smoothly with dose. In BTF, this translates to the prior belief that V_{jt} and $V_{j(t+1)}$ should be similar. To encode this, we place priors on the differences between dose-specific drug embeddings, rather than on the embeddings themselves,

$$(\Delta^{(k)} V_j)_\ell \sim \quad \text{MVN}(\mathbf{0}, \rho^2 \tau_{j\ell}^2 I)\,. \tag{2}$$

We call $\Delta^{(k)} \in \mathbb{R}^{L \times T}$ the composite trend filtering matrix; it contains all $(0, \ldots, k)$ trend filtering [23] matrices. The ordinary trend filtering matrix encodes only the $(k+1)^{\text{th}}$-order differences, implicitly assuming all lower-order differences are not smooth. The composite trend filtering matrix encodes all $(q+1)^{\text{th}}$-order differences for $q = 1, \ldots, k$. For example, the $k = 1$ case yields a prior on the first and second order differences,

$$\Delta^{(1)} = \begin{bmatrix} 1 & 0 & 0 & 0 & \ldots & 0 & 0 & 0 \\ 1 & -1 & 0 & 0 & \ldots & 0 & 0 & 0 \\ 0 & 1 & -1 & 0 & \ldots & 0 & 0 & 0 \\ & & & & \ldots & & & \\ 0 & 0 & 0 & 0 & \ldots & 0 & 1 & -1 \\ 1 & -2 & 1 & 0 & \ldots & 0 & 0 & 0 \\ 0 & 1 & -2 & 1 & \ldots & 0 & 0 & 0 \\ & & & & \ldots & & & \\ 0 & 0 & 0 & 0 & \ldots & 1 & -2 & 1 \end{bmatrix}. \tag{3}$$

The first line of eq. (3) places an independent prior on the first dose level in each drug, v_{j1}, to make the matrix non-singular and to ensure the prior is proper [21].

Column independence distinguishes functional matrix factorization from time-series tensor factorization [27, 19, 9, 20] where all columns are progressing through time together. In BTF, columns are evolving independently, though potentially with similar latent attributes. This independent evolution captures the notion that two drugs treated at the same concentration may have totally different effects due to the molecular size of the drug, its targeting receptor, and its chemical structure.

Global-local shrinkage priors. The variance parameters in eq. (2) control the smoothness of each curve. Small values of ρ^2 and $\tau_{j\ell}^2$ will shrink the $(j, \ell)^{\text{th}}$ difference to nearly zero, resulting in the curve being smoother; larger values enable the curve to jump in response to the data. BTF uses a global-local shrinkage model [16] where ρ^2 controls the smoothness of the entire matrix and $\tau_{j\ell}^2$ is a local shrinkage term for a specific drug at a specific dose. BTF places a horseshoe+ (HS+) prior [3, 1] on the shrinkage parameters,

$$\tau_{j\ell} \sim \text{C}^+(0, \phi_{j\ell}) \qquad \phi_{j\ell} \sim \text{C}^+(0, 1) \qquad \rho \sim P(\rho)\,. \tag{4}$$

The HS+ prior is asymptotic at zero and consequently shrinks most $\tau_{j\ell}$ values to nearly zero. However, it has heavy tails that decay very slowly. Thus, when the data suggests that a change in dose results in a sharp change in effect, the drug attributes are able to make sharp jumps. As noted by Bhadra et al. [1], a full Bayesian specification could choose a reasonable prior for ρ, such as a standard

Cauchy or Uniform$(0, 1)$. If an estimate of the number of non-zero entries is available, Van Der Pas et al. [24] make an asymptotic argument for setting $\hat{\rho}$ to the expected number of non-zeros. In practice, we find BTF is robust to the choice of global shrinkage parameter and instead perform a grid search over a handful of ρ values.

Posterior inference. Inference in BTF is performed through an efficient Gibbs sampler. The updates for the latent attributes depend on the form of $P(y_{ijt}; w_i^\top v_{jt})$, the likelihood function for sample i, treated with drug j, at dose t. Specifically, likelihoods fall into three categories: (i) Gaussian, for which updates are fully conjugate; (ii) binomial and related likelihoods, for which updates are conditionally conjugate through Pólya–Gamma augmentation; and (iii) black-box likelihoods, for which updates are non-conjugate. The derivations for the Gaussian and binomial categories are in appendices A and B, respectively; the horseshoe parameter updates are in appendix C. In the remainder of the paper, we focus on inference for non-conjugate likelihoods, as this is the category of observations for the Bayesian dose-response model in Section 4.

3 Generalized analytic slice sampling for black-box likelihoods

Posterior inference in BTF is done via Gibbs sampling. However, this requires us to be able sample from the conditional distributions for each of our parameters. For generic likelihoods, the conditional distributions of the latent attributes w_i and v_{jt} are typically not available in closed form. Moreover, the likelihood may impose hard constraints on the values of matrix entries. For instance, in Poisson factorization, the $w_i^\top v_{jt}$ corresponds to the Poisson rate of observed entries in the tensor, which must always be positive. In other cases, such as the dose-response model in Section 4, the inner product may parameterize a probability or percentile, requiring $w_i^\top v_{jt} \in [0, 1]$. A naive MCMC-within-Gibbs step with rejection sampling for invalid proposals will have a high rejection rate and lead to poor mixing. In this section, we present an exact approach for generic likelihoods that handles arbitrary linear constraints.

Sampling from the conditional distributions of the latent attributes can be reduced to the problem of sampling from the posterior of a vector x with a multivariate normal prior constrained by a set of linear inequalities,

$$x \sim P(y; x)\mathrm{MVN}(x; \mu, \Sigma)\mathbb{I}[Dx \geq \gamma] \,. \tag{5}$$

Slice sampling [15] samples from $P(x|y)$ by sampling over the augmented joint distribution $P(x, \epsilon \mid y)$ where $\epsilon = P(y \mid x)$. When the prior is an unconstrained multivariate normal, the augmentation can be done by noting that a multivariate normal forms an ellipse of equal probability. Elliptical slice sampling [14] samples from the posterior on x by sampling a candidate ellipse v from the prior and sampling an angle $\theta \in [-\pi, \pi]$ such that $x' = x\mathrm{cos}(\theta) + v\mathrm{sin}(\theta)$ and

Algorithm 1: Generalized analytic slice sampling (GASS) for constrained MVN priors

```
Data: Valid current point $x$, mean $\mu$, covariance $\Sigma$, log-likelihood $\mathcal{L}$,
      constraints $(D, \gamma)$
Result: MCMC sample from $P(x') \propto \exp(\mathcal{L}(x'))\mathrm{MVN}(x'; \mu, \Sigma)\mathbb{I}[Dx' \geq \gamma]$
$t = \mathcal{L}(x) + \log \epsilon, \qquad \epsilon \sim U(0, 1)$;
Sample proposal $v \sim \mathrm{MVN}(v; \mathbf{0}, \Sigma)$;
Grid approximation $\mathcal{G} = \mathrm{grid}(-\pi, \pi)$;
foreach constraint $(d_i, \gamma_i) \in (D, \gamma)$ do
    $a = d_i^\top(x - \mu)$, $b = d_i^\top v$, $c = \gamma_i - d_i^\top \mu$;
    if $a^2 + b^2 - c^2 \geq 0$ and $a \neq -c$ then
        Get $\theta_1, \theta_2$ as in eq. (6);
        if $a^2 > c^2$ then
            $\mathcal{G} = \mathcal{G} \bigcap [\theta_1, \theta_2]$;
        else
            $\mathcal{G} = \mathcal{G} \bigcap ([-\pi, \theta_1] \bigcup [\theta_2, \pi])$;
        end
    end
end
Generate candidate samples $\mathcal{X} = \{x' \colon x\cos(\theta_g) + v\sin(\theta_g) + \mu, \theta_g \in \mathcal{G}\}$;
Select uniformly from sufficiently likely candidates $\{x' \colon \mathcal{L}(x') \geq t, x' \in \mathcal{X}\}$.
```

$P(y; x') \geq P(y; x) \times u\,, u \sim U(0, 1)$. Adding constraints as in eq. (5) could be handled by pushing the constraints into the likelihood, but would result in high rejection rates.

We extend elliptical slice sampling to directly handle constrained multivariate normal priors. Our approach is a generalization of the analytic slice sampling procedure of Fagan et al. [6] for truncated multivariate normals. The key difference is that the original analytic slice sampler only considered centered truncated multivariate normals with no likelihood component. Generalizing this procedure to handle the more general case in eq. (5) introduces several edge cases.

Algorithm. The full GASS procedure is procedure is presented in Algorithm 1. Briefly, the idea of GASS is to note that the constraints can be pushed inside the proposal update. Given a single constraint requiring that our output point satisfies $d^\top x' \geq \gamma$, a valid angle θ must satisfy $a\cos\theta + b\sin\theta - c \geq 0$, where $a = d^\top(x - \mu)$, $b = d^\top(v - \mu)$, and $c = \gamma - d^\top \mu$. Basic trigonometry implies that the feasible range of θ is a subset of $[-\pi, \pi]$ whose boundary points are

$$\theta_1, \theta_2 \;=\; 2\mathrm{arctan}\left(\frac{b \pm \sqrt{a^2 + b^2 - c^2}}{a + c}\right). \tag{6}$$

Two cases cause the entire ellipse to be valid: (i) $(a^2 + b^2 - c^2) < 0$ and (ii) $a = -c$. In the first case, $a^2 + b^2 < c^2 \Rightarrow a\text{cos}\theta + b\text{sin}\theta > c$, for all θ. In the second case, the only place the constraint touches the ellipse is on the extremal point of the ellipse and thus its selection has probability zero. For all other cases, the subset is determined based on the sign of $a^2 - c^2$. A positive sign indicates the quadratic in the inequality is concave and eq. (6) defines the boundaries of a contiguous region; a negative sign indicates convexity and thus the complement of the interval. As our output sample may need to satisfy many such constraints, we can simply repeat the above process to find all the valid regions and take their intersection. We then numerically approximate the valid θ regions with a fine-grained 1D grid. Sampling is performed in a quasi-Monte Carlo fashion, uniformly over the valid grid points.

Conditioning heuristic. Elliptical slice sampling schemes like GASS can suffer from poor mixing when the likelihood overwhelms the prior. In this case, the angle of the ellipse will be very sharp, causing the sampler to have a small region of the posterior that it can jump to with non-negligible probability at each step. Fagan et al. [6] suggest using an expectation propagation for generic truncated normals. In the case of BTF, the prior parameters for W are a function of V, and vice versa. Thus, expectation propagation would need to be performed every iteration of the Gibbs sampler, which would considerably increase the computational cost of inference.

We instead approximate the entire functional matrix once at the start, by a constrained matrix factorization. This is fast as it only requires alternating between solving linear programs for the rows and columns. After fitting the rows and columns, we calculate an over-estimate of the variance, analogous to an EP approximation, as a multiple of the empirical squared error in the estimate for each column and row. BTF uses the pseudo-EP approximation at every step in the Gibbs sampler to calculate an adjusted prior, following the same updates as in the Gaussian likelihood case (see appendix A for details). The log-likelihood used in the GASS procedure is then the original log-likelihood minus the log-pseudo-EP likelihood, leaving the resulting distribution equivalent but increasing the range of admissible angles θ.

4 Bayesian dose-response modeling for cancer drug discovery studies

The BTF model is a general framework for functional matrix factorization. To apply this framework to dose-response data requires an extra set of modeling steps on top of BTF. Here we describe the drug experiments in detail and an empirical Bayes procedure to estimate the observation likelihood in the face of technical error.

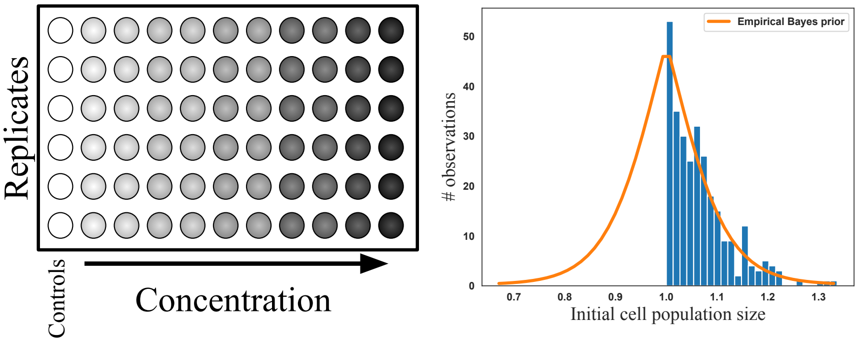

(a) Experimental design

(b) Empirical Bayes estimate

Figure 2: Left: The layout of each microwell plate experiment used to generate a single functional matrix entry. Cells are pipetted one column at a time, leading to correlated errors. Right: Estimate of the prior distribution of mean cell counts in each column, relative to the control column mean. The prior is estimated empirically assuming the lowest concentration had no effect if it had a higher mean.

Experimental design and technical error. Each functional matrix entry is derived from a microwell plate experiment where a one drug is tested against a one biological sample. Each experiment measures cell counts after applying the drug at 9 different concentrations. The cell counts are measured relative to a baseline control population where no drug was applied. For the control and each concentration level, 6 replicates are tested. Figure 2a shows the design of each 60-well plate experiment. All experiments are normalized by dividing the population size estimates at each concentration by the control mean for the plate.

The first step in each experiment is to pipette an initial population of cells into each of the 60 microwells on the plate. This is a time consuming process for the biologist, often taking hours to pipette a single plate. To speed up the plating process, biologists use a multi-headed pipette that enables them to simultaneously fill an entire column of each plate. This reduces the burden on the biologist, but comes at a cost: correlated errors.

When a biologist fills a microwell, they first draw a pool of cells into the pipette. Given the small volumes involved in laboratory experiments, the actual number of cells drawn can vary substantially on a relative basis. Using a multi-headed pipette transforms this variation into a hierarchical model: first a pool of cells is drawn into the pipette, then it is split among all the heads. The majority of the variation comes in the initial sampling, with small noise added in the splitting process. This has the unintended side effect of creating correlated errors between all microwells in a single column.

Empirical Bayes likelihood estimation. The correlated errors in the columns render the exact effects unidentifiable. Each column has two latent variables affecting the final population size of cells: a dose-level effect from the drug and an initial population size from the pipetting. Since both of these variables affect all replicates in a column, disentangling them precisely is impossible. Nevertheless, an estimate of dose-response must be provided.

We take an empirical Bayes approach to disentangling the variation in drug effects from the technical error in pipetting. In most experiments, the lowest concentration tested is too small to have any effect on cell survival. We therefore make the assumption that any experiment where the mean of the control replicates is lower than the mean of the replicates treated at the lowest concentration has effectively two sets of control columns. This enables estimation the variation between means and form an empirical Bayes prior for the pipetting error.

Specifically, we form a histogram of all lowest-concentration means greater than the control mean on the same plate. We then fit a Poisson GLM with 3 degrees of freedom to the histogram to estimate the prior probability that the mean of the initial population of cells was higher than the control mean. We then assume the true distribution is symmetric and obtain our empirical Bayes prior on the means. Figure 2b shows an example histogram and empirical Bayes prior estimate. The within-column variance is identifiable and estimated using the controls. The empirical Bayes likelihood is then a gamma mixture model that integrates out our uncertainty in the initial population mean,

$$P(y_{ijt} \mid w_i^\top v_{jt}) = \sum_{k=1}^{K} \left(\prod_{r=1}^{R} \hat{m}_k Ga(y_{ijtr}; \hat{a}_k, \hat{b}_k w_i^\top v_{jt}) \right) \mathbb{1}[0 \leq w_i^\top v_{jt} \leq 1] \,, \quad (7)$$

where $(\hat{m}, \hat{a}, \hat{b})_k$ are the weights derived from the empirical Bayes procedure. The scale regression form of the inner product is due to the property that the gamma random variable is being multiplied by the effect of the drug. That is, the population of cells is being killed at some latent rate. The inner product is constrained to be a proportion, as the drugs are known not to help any cells grow (i.e., the proportion must be at most 1) and a drug cannot kill more than all of the cells. The likelihood in eq. (7) is non-conjugate to the BTF hierarchical model and thus we use the generalized elliptical slice sampling routine from Section 3 for inference.

5 Results

We study BTF in two scenarios: (i) a dynamic matrix factorization with Poisson observations and (ii) a real cancer drug study. In both cases, we run 5 independent trials, holding out a different subset and report averages over all trials. BTF outperforms all baselines in terms of log probability on held out data for both benchmarks.

	Poisson Dynamical System			Cancer Drug Study	
	Observations	True rate			Observations
Model	NLL	MAE	RMSE	Model	NLL
NMF	437.32 ± 31.73	1.46 ± 0.32	2.26 ± 0.57	NMF	262.75 ± 308.12
PGDS	396.98 ± 11.86	1.24 ± 0.22	1.98 ± 0.40	LMF	589.17 ± 582.29
BTF	$\mathbf{369.91 \pm 7.66}$	$\mathbf{0.87 \pm 0.18}$	$\mathbf{1.24 \pm 0.28}$	BTF	$\mathbf{-80.22 \pm 9.67}$

Table 1: Mean results ± standard error on held out data in the benchmarks; smaller is better for all metrics. NMF: nonnegative matrix factorization; PGDS: Poisson-gamma dynamical system; LFM: logistic factor model; BTF: Bayesian tensor filtering (this paper).

Non-stationary Poisson dynamical systems. We benchmark BTF on a synthetic functional Poisson matrix dataset where the observations are Poisson distributed with a latent rate curve for each function. The rate at every point in the curve is the inner product of two gamma random vectors,

$$
\begin{aligned}
&h_{j\ell} \sim \text{Bern}(0.2)\,, \quad u_{j\ell d} \sim (1 - h_{j\ell})\delta_0 + h_{j\ell}\text{Ga}(1,1)\,, \quad v_{jtd} = \sum_{\ell=1}^{t} u_{j\ell d}\,, \\
&w_{id} \sim \text{Ga}(1,1)\,, \qquad\qquad\qquad y_{ijt} \sim \text{Pois}(\langle w_i, v_{jt}\rangle)\,.
\end{aligned}
$$

The resulting true rates form a monotonic curve of constant plateaus with occasional jumps. As in the dose-response data, the columns evolve independently of each other, rather than through a common time parameter. We set the latent factor dimension to 3.

We compare BTF to nonnegative matrix factorization (NMF) and the Poisson-gamma dynamical system (PGDS) model of Schein et al. [18]. We use the default parameters for PGDS; for BTF, we set $\rho^2 = 0.1$; both models use the true factor dimension 3. We run both BTF and PGDS for 2000 burn-in iterations and collect 2000 samples on an $11 \times 12 \times 20$ tensor with the upper left $3 \times 3 \times 20$ corner held out. We conduct 5 independent trials, regenerating new data each time and evaluating the models on the held out data. We measure performance in three metrics: mean absolute error (MAE) on the true rate, root mean squared error (RMSE) on the true rate, and negative log-likelihood (NLL) on held out observations. Table 1 (left) presents the results.

The PGDS model outperforms the NMF baseline, and BTF outperforms both methods. There are two possible reasons for the better performance of BTF relative to PGDS. First, the PGDS model uses a common "time" factor for all columns, but in our simulation columns evolve independently. Second, the large discrete jumps are not well-modeled by PGDS. In follow-up experiments, we found no improvement for PGDS from using larger factor sizes to potentially account for the first issue. This suggests the local adaptivity of BTF accounts for the better performance.

Cancer drug study. We evaluate our empirical Bayes dose-response model, built on top of BTF, on a cancer drug study. The study tested 35 drugs against 28 tumor samples, each at 9 different concentrations. The standard dose-response modeling approach in cancer datasets is a log-linear logistic model [25]. For a baseline, we extend that model to a logistic factor model (LFM), using the same preprocessing strategy; we also compare to NMF as a second baseline.

We run 5 independent trials, holding out 30 curves at random, subject to the constraint that no column or row is left without any observations in the training set. We choose the LFM factor size by 5-fold cross-validation on the training set. For BTF, we perform a grid search over hyperparameters: $\rho^2 = \{0.001, 0.01, 0.1\}$, factor size $D = \{1, 3, 5, 8\}$, and the order of the trend filtering matrix $k = \{0, 1\}$; we select the best model using the deviance information criterion [4].

Table 1 (right) present the results. BTF outperforms both baselines in terms of NLL. Furthermore, the BTF procedure is also more stable, with a much lower reconstruction variance than either baseline. This suggests BTF not only forms a more accurate basis for a dose-response model, but is also more reliable.

6 Conclusion

We presented Bayesian Tensor Filtering, a hierarchical Bayesian model for functional matrix factorization. BTF uses locally-adaptive shrinkage priors to encourage smoothness in the functions while still allowing for sharp discontinuities. We derived a Gibbs sampling inference procedure for BTF, including a new slice sampling technique for constrained multivariate normal priors with non-conjugate likelihoods. BTF was then used as the basis for a new dose-response model for multi-drug, multi-sample studies. Finally, on both simulated and real data benchmarks, the BTF-based models better reconstructed held out data in comparison to state-of-the-art models.

References

[1] Anindya Bhadra, Jyotishka Datta, Nicholas G. Polson, and Brandon Willard. The horseshoe+ estimator of ultra-sparse signals. *Bayesian Analysis*, 12(4):1105–1131, 2017.

[2] Anindya Bhadra, Jyotishka Datta, Yunfan Li, and Nicholas G Polson. Horseshoe regularization for machine learning in complex and deep models. *arXiv preprint arXiv:1904.10939*, 2019.

[3] Carlos M. Carvalho, Nicholas G. Polson, and James G. Scott. The horseshoe estimator for sparse signals. *Biometrika*, 97(2):465–480, 2010.

[4] Gilles Celeux, Florence Forbes, Christian P. Robert, and D. Michael Titterington. Deviance information criteria for missing data models. *Bayesian Analysis*, 1(4): 651–673, 2006.

[5] Jarno Drost and Hans Clevers. Organoids in cancer research. *Nature Reviews Cancer*, 2018.

[6] Francois Fagan, Jalaj Bhandari, and John Cunningham. Elliptical slice sampling with expectation propagation. In *Uncertainty in Artificial Intelligence*, 2016.

[7] James R. Faulkner and Vladimir N. Minin. Locally adaptive smoothing with Markov random fields and shrinkage priors. *Bayesian Analysis*, 13(1):225, 2018.

[8] Mathew J. Garnett, Elena J. Edelman, Sonja J. Heidorn, Chris D. Greenman, Anahita Dastur, King Wai Lau, Patricia Greninger, I. Richard Thompson, Xi Luo, Jorge Soares, et al. Systematic identification of genomic markers of drug sensitivity in cancer cells. *Nature*, 483(7391):570, 2012.

[9] Laetitia Gauvin, André Panisson, and Ciro Cattuto. Detecting the community structure and activity patterns of temporal networks: A non-negative tensor factorization approach. *PLoS one*, 9(1), 2014.

[10] P. Richard Hahn, Jingyu He, and Hedibert Lopes. Bayesian factor model shrinkage for linear IV regression with many instruments. *Journal of Business & Economic Statistics*, 36(2):278–287, 2018.

[11] Lei Huang, Shengnan Wu, and Da Xing. High fluence low-power laser irradiation induces apoptosis via inactivation of Akt/GSK3β signaling pathway. *Journal of Cellular Physiology*, 226(3):588–601, 2011.

[12] D. R. Kowal, D. S. Matteson, , and D. Ruppert. Dynamic shrinkage processes. *Journal of the Royal Statistical Society: Series B (Statistical Methodology)*, 2019.

[13] Enes Makalic and Daniel F. Schmidt. A simple sampler for the horseshoe estimator. *IEEE Signal Processing Letters*, 23(1):179–182, 2015.

[14] Iain Murray, Ryan Adams, and David MacKay. Elliptical slice sampling. In *Artificial Intelligence and Statistics*, 2010.

[15] Radford M Neal. Slice sampling. *The Annals of Statistics*, 31(3):705–767, 2003.

[16] Nicholas G. Polson and James G. Scott. Shrink globally, act locally: Sparse Bayesian regularization and prediction. *Bayesian Statistics*, 9:501–538, 2010.

[17] Nicholas G. Polson, James G. Scott, and Jesse Windle. Bayesian inference for logistic models using Pólya–Gamma latent variables. *Journal of the American Statistical Association*, 108(504):1339–1349, 2013.

[18] Aaron Schein, Hanna Wallach, and Mingyuan Zhou. Poisson-gamma dynamical systems. In *Advances in Neural Information Processing Systems*, 2016.

[19] Stephan Spiegel, Jan Clausen, Sahin Albayrak, and Jérôme Kunegis. Link prediction on evolving data using tensor factorization. In *Pacific-Asia Conference on Knowledge Discovery and Data Mining*, 2011.

[20] Koh Takeuchi, Hisashi Kashima, and Naonori Ueda. Autoregressive tensor factorization for spatio-temporal predictions. In *International Conference on Data Mining*, 2017.

[21] Wesley Tansey, Alex Athey, Alex Reinhart, and James G. Scott. Multiscale spatial density smoothing: An application to large-scale radiological survey and anomaly detection. *Journal of the American Statistical Association*, 112(519):1047–1063, 2017.

[22] Wesley Tansey, Kathy Li, Haoran Zhang, Scott W. Linderman, Raul Rabadan, David M. Blei, and Chris H. Wiggins. Dose-response modeling in high-throughput cancer drug screenings: A case study with recommendations for practitioners. *arXiv preprint arXiv:1812.05691*, 2018.

[23] Ryan J. Tibshirani. Adaptive piecewise polynomial estimation via trend filtering. *The Annals of Statistics*, 42(1):285–323, 2014.

[24] Stéphanie L. Van Der Pas, Bas J.K. Kleijn, and Aad W. Van Der Vaart. The horseshoe estimator: Posterior concentration around nearly black vectors. *Electronic Journal of Statistics*, 8(2):2585–2618, 2014.

[25] Daniel J. Vis, Lorenzo Bombardelli, Howard Lightfoot, Francesco Iorio, Mathew J. Garnett, and Lodewyk FA Wessels. Multilevel models improve precision and speed of IC50 estimates. *Pharmacogenomics*, 17(7):691–700, 2016.

[26] John N. Weinstein, Eric A. Collisson, Gordon B. Mills, Kenna R. Mills Shaw, Brad A. Ozenberger, Kyle Ellrott, Ilya Shmulevich, Chris Sander, Joshua M. Stuart, and Cancer Genome Atlas Research Network. The cancer genome atlas pan-cancer analysis project. *Nature Genetics*, 45(10):1113, 2013.

[27] Liang Xiong, Xi Chen, Tzu-Kuo Huang, Jeff Schneider, and Jaime G. Carbonell. Temporal collaborative filtering with Bayesian probabilistic tensor factorization. In *International Conference on Data Mining*, 2010.

[28] Aonan Zhang and John Paisley. Deep Bayesian nonparametric tracking. In *International Conference on Machine Learning*, pages 5828–5836, 2018.

A Gaussian likelihood

When the likelihood is normal, $y_{ijt} \sim \mathcal{N}(w_i^\top v_{jt}, \nu^2)$, where ν^2 is a nuisance parameter, the factor and loading updates are conjugate. Let $\tilde{V} = (v_{1,1}, v_{1,2}, \ldots, v_{1,T}, v_{2,1}, \ldots, v_{M,T})$, and $\Omega^{-1} = \mathrm{diag}\{1/\nu^2\}$, then the updates are multivariate normal,

$$\begin{aligned} Q^{(i)} &= (\tilde{V}^T \Omega^{-1} \tilde{V} + \mathrm{diag}(\sigma^{-2}))^{-1} \\ (w_i \mid -) &\sim \mathrm{MVN}\left(Q^{(i)} \tilde{V}^\top \Omega^{-1} \mathrm{vec}(Y_i^\top), Q^{(i)}\right) \\ \mathcal{T}^{(j)} &= \mathrm{diag}(1/(\rho^2 \tau_j^2)) \\ \Sigma^{(j)} &= (I_D \otimes \Delta^\top \mathcal{T} \Delta) + (W \otimes I_T)^\top \Omega^{-1} (W \otimes I_T) \\ (\mathrm{vec}(V_j) \mid -) &\sim \mathrm{MVN}(\Sigma^{(j)} (W \otimes I_T) \Omega^{-1} \mathrm{vec}(Y_{\cdot j}^\top), \Sigma^{(j)}) \,, \end{aligned} \tag{8}$$

where `diag` diagonalizes the given vector, `vec` is the vectorization operator, and $\otimes$ is the Kronecker product. In both the w_i and V_j updates the precision matrices will be sparse, making sampling from the conditionals computationally tractable.

B Binomial and related likelihoods via Pólya–Gamma augmentation

When the likelihood is binomial, $y_{ijt} \sim \mathrm{Bin}(n_{ijt}, 1/\{1 + e^{w_i^\top v_{jt}}\})$, where n_{ijt} is a nuisance parameter, the updates are conditionally conjugate given a Pólya–Gamma (PG) latent variable sample [17],

$$(\psi_{ijt} \mid -) \sim \mathrm{PG}(n_{ijt}, w_i^\top v_{jt}) \,, \qquad (w_i \mid -) \sim N(m_{\psi_i}, \Sigma_{\psi_i}) \,, \tag{9}$$

where $\Sigma_{\psi_i} = (\tilde{V}^\top \Psi_i \tilde{V} + \sigma^{-2} I)^{-1}$, $m_{\psi_i} = \Sigma_{\psi_i} \tilde{V}^\top \kappa$, $\Psi_i = \mathrm{diag}(\psi_{(i,1,1)}, \ldots, \psi_{(i,M,T)})$, and $\kappa = (y_{(i,1,1)} - n_{(i,1,1)}/2, \ldots, y_{(i,M,T)} - n_{i,M,T}/2)$. The updates for V follow analogously. PG augmentation can be applied to binomial, Bernoulli, negative binomial, and multinomial likelihoods, among others.

C Local shrinkage updates

The local shrinkage parameters $\tau_{j\ell}$ can be updated through a double latent variable augmentation trick,

$$\begin{aligned}(\tau_{j\ell} \mid -) \sim & \quad \text{InvGamma}(D+1, \left|\left|\Delta^{(k)} V_j\right|\right|_2^2 /2 + 1/c_{j\ell}) \\ (c_{j\ell} \mid -) \sim & \quad \text{InvGamma}(1, 1/\tau_{j\ell}^2 + 1/\phi_{j\ell}) \\ (\phi_{j\ell} \mid -) \sim & \quad \text{InvGamma}(1, 1/c_{j\ell} + 1/\eta_{j\ell}) \\ (\eta_{j\ell} \mid -) \sim & \quad \text{InvGamma}(1, 1/\phi_{j\ell} + 1)\,. \end{aligned} \tag{10}$$

The updates in eq. (10) come from the HS+ prior being a two-level horseshoe prior. The inverse-gamma latent variable augmentation for the horseshoe is fast and typically mixes quickly [13].